Computational modelling of convective heat transfer in a simulated engine cooling gallery

K Robinson*, **M Wilson**, **M J Leathard**, and **J G Hawley**
Department of Mechanical Engineering, University of Bath, Bath, Avon, UK

Abstract: Experimental data from internal combustion (IC) engines suggests that the use of proprietary computational fluid dynamics (CFD) codes for the prediction of coolant-side heat transfer within IC engine coolant jackets often results in underprediction of the convective heat transfer coefficient. An experimental and computational study, based on a coolant gallery simulator rig designed specifically to reproduce realistic IC engine operating conditions, has been conducted to explore this issue.

It is shown that the standard 'wall function' approach normally used in CFD models to model near-wall conditions does not adequately represent some features of the flow that are relevant in convective heat transfer. Alternative modelling approaches are explored to account for these shortcomings and an empirical approach is shown to be successful; however, the methodology is not easily transferable to other situations.

Keywords: convective heat transfer, computational fluid dynamics, internal conbustion engines

1 INTRODUCTION

Computational fluid dynamics (CFD) has been in regular use for approximately the last 15 years for the analysis of industrial fluid flow problems. One such application is the simulation of flow within the coolant passages of internal combustion (IC) engines in order to predict the pressure drop and the spatial distributions of the coolant velocity and heat transfer coefficient. These predictions can then be used as coolant-side boundary conditions for finite element (FE) analyses of engine components to predict operating temperatures. Alternatively the combined fluid flow–metal conduction problem can be solved iteratively as a 'conjugate' heat transfer problem, in which the solid regions are modelled within the CFD code with cells with zero flow, or as a coupled FE–CFD analysis as described by Ennemoser *et al.* [**1**]. Coolant flow analysis has, however, traditionally

been performed isothermally, i.e. the heat transfer is not modelled directly and heat transfer coefficients are inferred semiempirically from near-wall velocity profiles and turbulence levels [**1–3**].

Most flows of practical engineering interest are turbulent, and turbulent mixing then usually dominates the behaviour of the flow. For engine coolant flows, the most popular computational model for turbulence is the k–ε model (where k is the kinetic energy per unit mass of fluid arising from the turbulent fluctuations in the velocity and ε is the rate at which the turbulent kinetic energy is dissipated to smaller eddies). This and other such 'two-parameter' models are used widely as they do not require geometric or flow-specific inputs and are therefore relatively easy to incorporate into solution procedures.

The coolant space is divided in a CFD model into individual solution cells, and three-dimensional discretized equations for the conservation of mass, momentum, and energy can be solved iteratively in each cell to determine the flow distribution subject to the boundary conditions imposed. The size of the cells is prescribed to give the required level of

* *Corresponding author: Department of Mechanical Engineering, University of Bath, Claverton Down, Bath, Avon, BA2 7AY, UK. email: enskr@bath.ac.uk*

resolution in different areas of the model. Typically, a finer mesh would be specified in the anticipated critical regions.

Modelling coolant flow in IC engines as outlined above has proved successful in allowing engineers to develop engine cooling strategies to ensure high coolant heat transfer in critical areas. Using this approach, engine design features such as the size of coolant transfer holes in the head gasket are tuned with the aid of CFD predictions to achieve experience-based velocity targets in thermally critical areas. The success of this approach results from the high degree of confidence associated with the CFD velocity prediction [4, 5] and, where high velocities are present, high rates of convective heat transfer naturally follow. However, it has been shown that the actual heat transfer coefficients are often significantly under-predicted [6–8]. Where appropriate experimental data exist, it has become user practice to increase heat transfer coefficients manually to bring them in line with experimentally observed values. However where no such data exist, the predictions need to be treated with some caution.

An experimental rig study has been undertaken to explore the issue of heat transfer measurement and prediction in the context of IC engine cooling passages, and experimental results and empirical modelling approaches from this work for aspects of nucleate boiling behaviour have been reported previously [6–8]. In the present paper, the issue of modelling the convective heat transfer using computational methods is explored.

2 THE EXPERIMENTAL RIG

Following an analysis of the previous experimental work of others [9], the rig was designed to simulate as far as is practical the mechanisms of heat transfer under on-engine conditions. Many previous rigs have used long tubular ducts with axisymmetrically heated smooth surfaces and pure water coolants and attempted to relate data from such rigs to engine cylinder blocks and heads. In this study, on-engine conditions were more closely replicated by using a short rectangular duct (16 mm wide and 10 mm high) heated on the underside only, to simulate conditions in a cylinder head cooling passage. A rough (sand-cast) heating surface and actual engine coolant formulations were used and a schematic diagram of the rig is shown in Fig. 1.

The rig was designed to accommodate test pieces of different surface finishes, materials, and inlet and outlet geometries [9]. Provision was made to regulate independently the system pressure, temperature, coolant flow velocity, and heat flux over a range of conditions representative of engine cooling systems, as shown in Table 1. These conditions correspond to a Reynolds number range from 3485 to 69 744 based on the hydraulic diameter of the duct and a bulk coolant temperature of 90 °C.

Glass plates were used to form the sides of the duct to allow optical access to observe bubble nucleation, growth, development, and detachment which would assist interpretation of the measured data under convective flow boiling conditions.
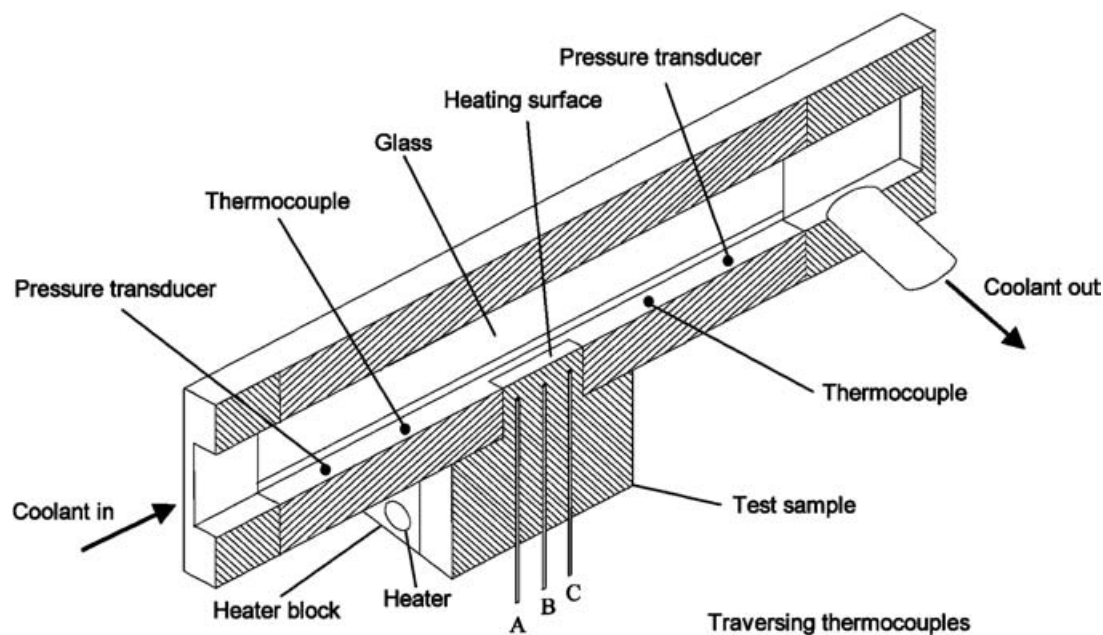

Fig. 1 Simulated engine cooling gallery

Table 1 Experimental parameters and ranges

Test variable	Variation
Heat flux	0–2.0 MW/m²
Bulk coolant velocity	0.25–5.0 m/s
Pressure	1–3 bar absolute
Coolant temperature	60–120 °C
Surface finish	As cast, machined smooth

The metal test sample was heated by four electric cartridge heaters embedded in two copper blocks which were clamped to the sides of the test sample. The dimensions of the heated surface were 10 mm wide by 50 mm long. The heat flux into the test sample was incremented in small steps and the rig was allowed to reach a steady state. At each test point, the heat flux–surface temperature relationship was established by measuring the temperature gradient through the test sample using traversing K-type thermocouples. The thermocouples at all three locations shown were traversed along the heat flow axis to within 2 mm of the heat transfer surface. The heat flux at each location was deduced as the product of the temperature gradient and metal thermal conductivity, whilst the surface temperature was calculated by a small extrapolation of the temperature gradient.

Experiments were performed using both smooth and 'as-cast' test pieces. The test pieces were manufactured using an aluminium alloy and manufacturing process identical with that used to produce engine cylinder heads. The smooth test pieces were machine finished whereas the as-cast test pieces were left unfinished.

A form Talysurf was used to study the surface finish of the test pieces. It was found that the R_a value of the as-cast surface was an average of 12.4 μm. The R_a value represents the average of absolute values of deviations of the surface from a mean surface height [10]. For the as-cast test piece surface a roughness Reynolds number $Re_k = \rho u_\tau k_s/\mu = 12$ was determined. This is in the transitional roughness region according to Nikuradse [11].

3 CFD MODEL OF THE EXPERIMENTAL RIG

The fluid flow was established to be turbulent under the experimental conditions outlined above and was modelled using a k–ε turbulence model in conjunction with a wall function approach. The commercial (finite volume) CFD code STAR-CD was used to solve the corresponding three-dimensional steady flow and energy equations. A non-linear (quadratic) form of the

k–ε model was used throughout the study described here, as it provides a more realistic prediction of the turbulent flow near the corners of a rectangular duct. Although the region around the test piece is of primary interest, it was necessary to incorporate the sections upstream of the heated section in order to allow the flow profile entering the main duct from the inlet sections to be represented.

Two techniques are available to model boundary layer flows, requiring different grid resolutions near the wall as illustrated in Fig. 2. The first option known as 'wall functions' (Fig. 2(a)) makes use of the universal nature of many fully turbulent boundary layers to describe the velocity, shear stress, turbulence energy and thermal profiles close to the wall but outside the viscous sublayer (for $30 < y^+$ and $y/\delta < 0.3$) using semiempirical relationships calibrated in simple two-dimensional flows [12], for which the velocity and wall shear stress can be shown to be related by [2]

$$u^+ = \frac{1}{\kappa} \ln y^+ + B = \frac{1}{\kappa} \ln(Ey^+) \tag{1}$$

where E is a wall roughness parameter and where $11 < y^+ < 250$ approximately. Experimental data suggest that $\kappa = 0.41$ and that, for smooth walls, $B = 5.5$ (giving $E = 9.5$) [13].

The use of so-called 'wall functions' as described above avoids the need to employ an extremely fine mesh to resolve the turbulent boundary layer explicitly and is therefore computationally efficient. However, the formulae used for the wall functions are based upon a set of assumptions about the flow strictly valid for only fully developed flow but which may reasonably approximate the conditions encountered in many boundary layer flow situations. Apsley and Leschziner [14] commented that wall functions are inherently inferior to a full calculation of the boundary layer, and Wilcox [15] noted that, under conditions such as strong pressure gradients, separated and
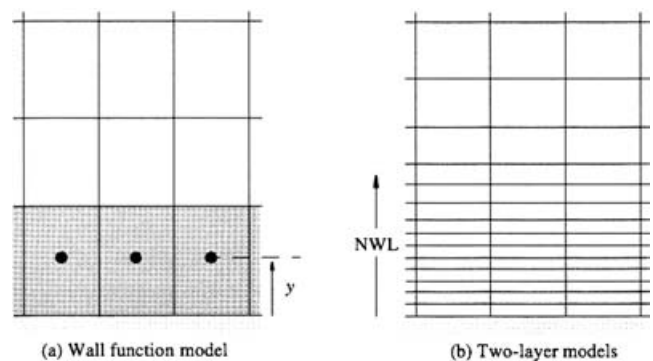

Fig. 2 Near-wall-boundary-layer modelling (NWL, near-wall layer)

impinging flows, the accuracy of the wall function approach can be poor.

The second boundary layer modelling option as illustrated in Fig. 2(b) is to use a near-wall layer, i.e. a mesh that is fine enough close to the wall to allow turbulence model equations to be solved across the boundary layer right up to the wall. Since the region very close to the wall ($y^+ < 5$) is dominated by viscous effects a turbulence model that includes low-Reynolds-number turbulence behaviour is required [16]. This method resolves the boundary layer realistically at the expense of a large increase in the number of computational cells compared with the wall function approach.

4 COOLING GALLERY COMPUTATIONS

4.1 Wall function results

The mesh used for the CFD model of the full experimental rig is shown in Fig. 3. The effect of the near-wall cell size on the prediction of heat transfer coefficient along the heated test piece was investigated for the model. It was found that the predicted values of heat transfer coefficients did not vary significantly for y^+ values greater than 30 using the wall function technique. A mesh having ten cells in the vertical direction and 12 cells in the horizontal direction was used subsequently, giving values for y^+ greater than 30 and less than 100 for the entire test section and a value of y^+ of around 40 at the test piece. The heat flux to the test section and inlet fluid temperature measured on the experimental rig [9] were used to provide the thermal boundary condition in the computations. Normalized global residuals for each solution variable were reduced to below 10^{-5} by the end of the iterative numerical solution, ensuring that the computations had converged.

Insensitivity of the results to prescribed inlet boundary conditions was confirmed by using two different conditions at the inlet: a uniform and a fully developed velocity profile. It was found that this made no difference to the velocity distributions in the test section, and as such the results can be assumed to be independent of the inlet boundary condition. The outlet boundary condition is sufficiently far from the test section to ensure that this boundary also has no effect on the flow profiles predicted at the test piece location.

The sensitivity of the results to the prescribed value of turbulence intensity at the inlet was also considered. The value at inlet was varied between 1 and 6 per cent, as suggested by Versteeg and Malalasekera [2] for pipe flow. It was found that there was a negligible effect on the velocity profiles produced in the region of the test piece, resulting in a negligible variation in heat transfer coefficient.

The heat transfer coefficients predicted under rig test conditions using the smooth surface wall function approach and the k–ε turbulence model are shown in Fig. 4 in comparison with experimental results. The large underprediction of the measured values by the CFD model is clearly seen. The vertical bars on the experimental results graph show the range of
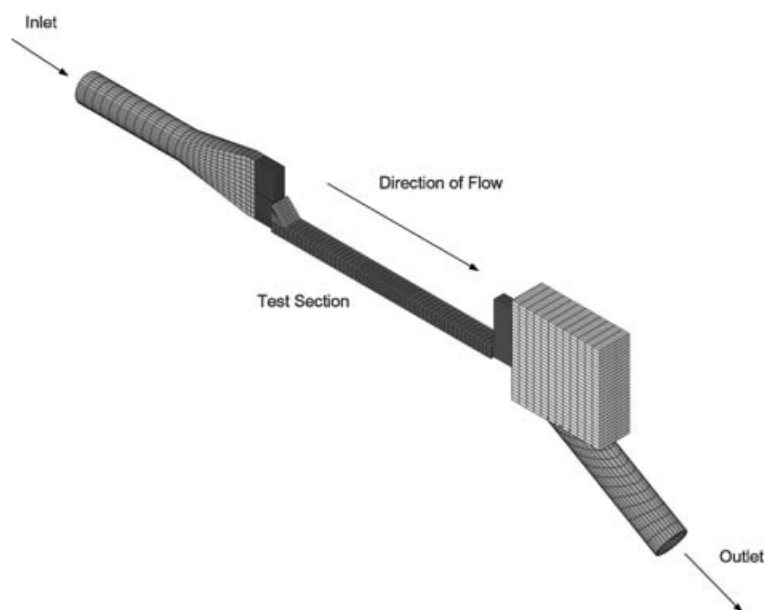

Fig. 3 CFD model of simulated engine cooling gallery rig

Proc. IMechE Vol. 221 Part D: J. Automobile Engineering

JAUTO450 © IMechE 2007

Heat transfer coefficient variation with velocity
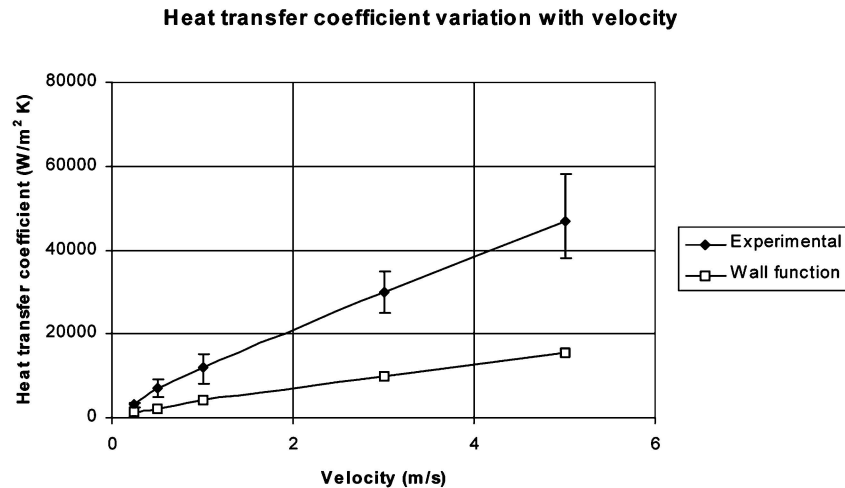

Fig. 4 Comparison of experimental and wall function predicted heat transfer coefficient versus velocity

heat transfer coefficients measured as a result of different coolant inlet temperatures.

The heat transfer process is essentially controlled by the very thin interface between the coolant and heated wall rather than the bulk of the fluid, i.e. the same region modelled by the wall function. The modelling of the heat transfer coefficient is therefore completely dependent on the assumptions implicit in the wall function approximation. Using the wall function approach, the growth of the hydrodynamic boundary layer is not modelled, and hence the heat transfer enhancement (relative to the developed flow case) due to the thinner boundary layer of undeveloped flow is also not represented. The highly irregular shape of engine cooling passages dictates that the flow will be very different from the idealized flow of regular ducts and rarely, if ever, have the opportunity to become fully developed. Thus there is a very significant difficulty for any modelling approach which relies on wall functions.

In order to assess the importance of the turbulence model on the computed flow in the rectangular cooling gallery, a separate CFD model was developed for fully developed flow in a rectangular duct having the same geometry as the simulated engine cooling gallery test section. The model consisted of a duct 16 mm wide, 10 mm high, and 500 mm long. The flow conditions and inlet turbulence parameters were chosen to be the same as those in the cooling gallery model, and the computed velocity profile did not vary significantly with downstream distance towards the end of the duct, indicating that the flow had become fully developed. The heat transfer coefficients obtained from the wall function CFD model for a range of velocity values for this fully developed flow situation were in excellent agreement with the

empirical correlation for fully developed flow in smooth pipes due to Dittus and Boelter (DB) [**17**] and given by

$$Nu = 0.023 \, Re^{0.8} \, \mathrm{Pr}^{1/3} \tag{2}$$

confirming that the wall function method operates correctly for this case.

A low-Reynolds-number version of the turbulence model was also tested for the fully developed flow situation. The largest near-wall cell size that could be used (to give heat transfer coefficients not depending on the grid) was found to be 0.025 mm for the 1 m/s case and 0.0125 mm for the 3 m/s case, the difference being due to the requirement that y^+ be equal to approximately 1. For the 3 m/s velocity, the low-Reynolds-number quarter-model required around 30 times the number of cells in the direction perpendicular to the wall compared with the equivalent wall function model. Thus, although the important effects of developing flow would be likely to be captured using a low-Reynolds-number model, and although recommendations are available to incorporate surface roughness effects through the wall boundary conditions for turbulence quantities (see, for example, reference [**18**]), the computational demand makes this method unattractive for application to realistic engine cooling gallery configurations, where the low-Reynolds-number treatment might be required to compute the heat transfer for more than one wall of each duct passage.

4.2 Velocity profile

Figure 5 shows the computed velocity profile at the centre of the heated test piece for the 1 m/s case. The fluid flows into the entry region, past the 45°
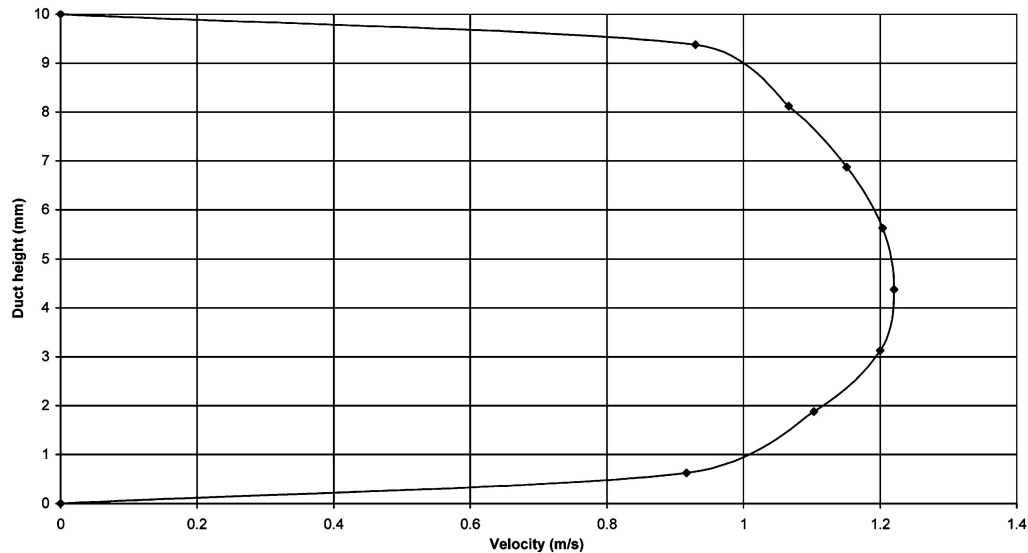
Fig. 5   Velocity profile at the centre of the heated test piece (1 m/s average velocity)

angle, travels through the test section, and exits into the mixing box before leaving through the outlet pipe. The bias in the flow towards the bottom deck arises because the flow is forced into the test section through the 45° angled inlet, and the profile is still developing when the flow reaches the test section. The boundary layer is shown by the sharp increase in velocity between the first and last points and the wall values (zero velocity). No direct information is available to validate the computed velocity profile; however, other work has shown that velocity profiles in IC engine cooling components can be predicted accurately by CFD models using wall functions [**4**, **5**, **19**].

The development length required for fully developed flow to become established along a duct is given by [**20**]

$$10 < \frac{x}{D} < 60 \qquad (3)$$

where x is the distance along the duct at which the flow becomes fully developed and D is the hydraulic diameter. The configuration 10 mm high and 16 mm wide for the duct in the present work results in an x/D ratio of 6.987 and 9.425 for the A and C thermocouple positions respectively, both less than that required for fully developed flow to be expected.

As the velocity profile is still developing, it is informative to determine where the profile is predicted to become fully developed. Equation (3) suggests the flow to become fully developed somewhere between 123 mm and 738 mm along the duct. The location between these two values will depend largely on the entrance geometry to the duct. Since

in this case there is a fairly abrupt entry, it is possible that the fluid will require a large distance before becoming fully developed.

4.3   Surface roughness

The effect of surface roughness was considered, for the 1 m/s case only, by using a different value of E in equation (1). The roughness Reynolds number $Re_k = 12$ for the as-cast test piece (section 2) results in a value of 9.8 for the constant B [**13**], and equation (1) was used to specify a value for the corresponding constant E in computations.

Changing the value of E from the default value for a smooth surface to the rough surface value for the engine cooling gallery simulator increased the predicted heat transfer coefficient by 30 per cent, from 4084 W/m² K to 5343 W/m² K.

The measured heat transfer coefficient at 1 m/s was 8400 W/m² K for the smooth surface and 11 000 W/m² K for the as-cast surface. These are average values over the convection region for the appropriate test conditions. This is an increase in heat transfer coefficient of 32 per cent due to surface roughness. The change in heat transfer coefficient due to roughness effects is therefore reproduced well by the wall function CFD model; however, the absolute values of heat transfer coefficient are significantly lower than the experimental results.

4.4   Fluid temperature

Figure 6 shows the variation in the fluid temperature profile through the test section. In this case the coolant inlet temperature is 90 °C. Heat is applied
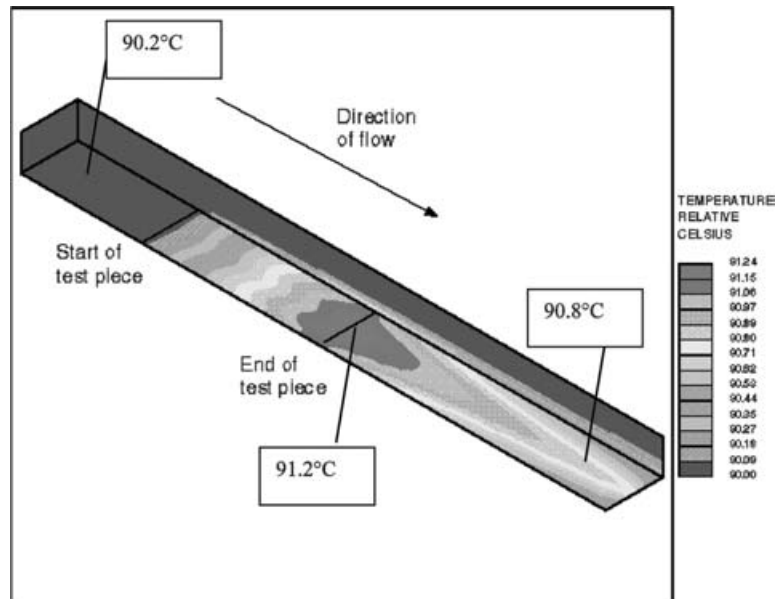
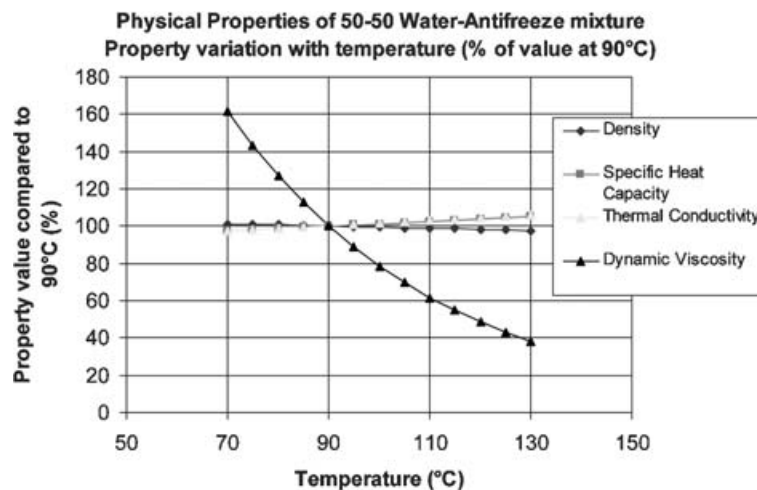**Fig. 6** Temperature profile through the test section

Fig. 7 Coolant (50–50 water–antifreeze mixture) property variation with temperature (percentage of the value at 90 °C)

only to the test piece surface. The fluid temperature rises along the test piece and then, as no more heat is being added to the fluid, the temperature drops along the rest of the test section. In this case there is only a small temperature rise, 1.4 °C. It was found that for conditions of 60 °C fluid temperature at the inlet, with strong heating, the coolant temperature could rise by as much as 10 °C.

The isothermal CFD model used here did not account for fluid properties that vary with temperature. Of the fluid properties of the coolant used in this study, it has been determined by Robinson and co-workers [6, 9] that only the viscosity has a strong dependence on temperature, as shown in Fig. 8.

The relationship for the dependence of the dynamic viscosity μ (kg/ms) on the temperature T (°C) which has been curve-fitted to experimental results, is

$$\mu = 0.0065\, e^{-0.0241T} \tag{4}$$

This shows that the viscosity has a much higher sensitivity to temperature than the other physical properties relevant to heat transfer. A reduced viscosity will result in improved heat transfer as the turbulent mixing of the fluid will be greater, together with a thinner fluid dynamic boundary layer [20].

Figure 6 also illustrates the important point that the fluid dynamic and thermal boundary layers do not start at the same location. With reference to Fig. 1,
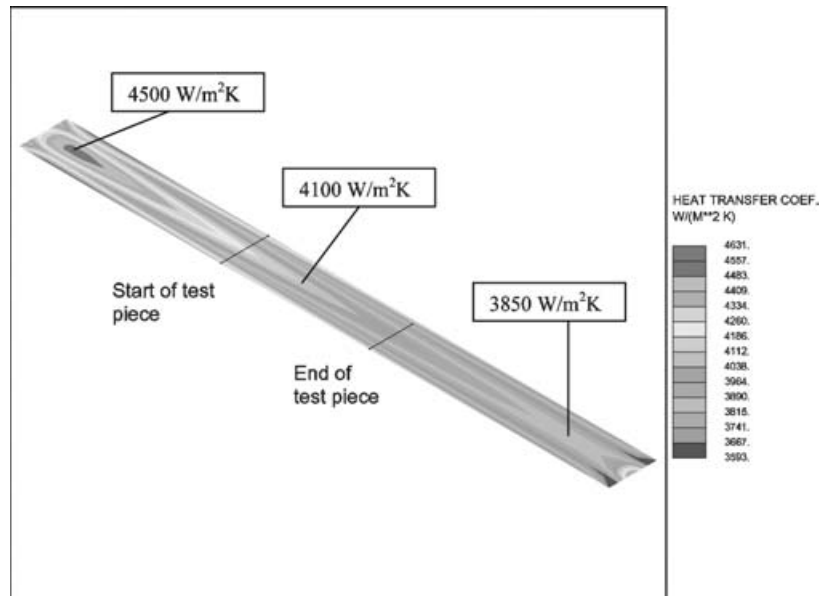
Fig. 8 Heat transfer coefficient profile along the test section floor

the fluid dynamic boundary layer begins to develop as soon as the fluid enters the duct, but the thermal boundary layer starts to develop later, as the fluid has to travel some distance before flowing over the central portion of the duct which contains the heated surface. This results in the effect known as an 'unheated starting length', shown by Robinson and co-workers [**6**, **9**] to result in underpredicted heat transfer if this effect is not accounted for. As the heat transfer coefficient predicted by the CFD code has no reliance on temperature, this effect will not be accounted for.

4.5 Heat transfer coefficient

Figure 8 shows the computed convective heat transfer coefficient plotted along the test section for a 1 m/s velocity. The development of the heat transfer coefficient as the fluid travels along the duct is clearly shown. The high heat transfer arising because the fluid is forced through the angled inlet section is indicated by the high heat transfer coefficient near the inlet.

Figure 4 shows how the heat transfer coefficient varies with velocity for the experimental and CFD results. The computed heat transfer coefficient is significantly lower than the measured values, about one third to one half for this velocity range. The underprediction is likely to be due to the developing nature of both the thermal and the fluid dynamic boundary layers, which are not accounted for by the wall function method. These results are consistent with the results obtained by Robinson and co-workers [**6**, **9**], who found that empirical algorithms

for fully developed flow, such as those developed by DB, also significantly underpredicted the measured heat transfer coefficients.

5 AN EMPIRICAL APPROACH

An alternative to using the low-Reynolds-number turbulence model approach to improve the predictive accuracy of the CFD model in these circumstances was to implement an empirical algorithm previously developed by Robinson and co-workers and described in detail elsewhere [**4**, **5**, **20**]. This was based on the standard empirical correlation for fully developed flow in smooth pipes due to DB, as given in equation (2), augmented by four factors which represented specific features of the test rig as follows.

1. *The fluid dynamic entry length.* The flow is not fully developed over the heated sample.
2. *The unheated starting length.* The heat transfer begins at a length downstream of point where the velocity boundary layer begins to develop.
3. *The rough surface of the heated sample.* This increases turbulence close to the wall and provides an increased surface area relative to a smooth surface.
4. *The sensitivity of the fluid viscosity to fluid temperature.* The near-wall fluid has a higher temperature and lower viscosity than the bulk.

Combining these four factors with the DB expression leads to a 'composite convection model'

given by

Nusselt number = (DB correlation)

$\times$ (entrance factor)

$\times$ (unheated starting length factor)

$\times$ (roughness factor)

$\times$ (viscosity loading factor)

or

$$Nu = (0.023\,Re^{0.8}\,Pr^{0.4})\frac{1 + 23.99\,Re^{-0.23}(x/D_{\mathrm{h}})^n}{[1 - (x_0/x)^{9/10}]^{1/9}}$$

$$\times \left[0.091\left(\frac{\varepsilon}{D_{\mathrm{h}}}\right)^{-0.125} Re^{0.363(\varepsilon/D_{\mathrm{h}})^{0.10}} \right]\left(\frac{\mu_{\mathrm{bulk}}}{\mu_{\mathrm{wall}}}\right)^{0.14}$$

$$(5)$$

where

$$n = 2.08 \times 10^{-6}\,Re - 0.815$$

with all properties evaluated at the film temperature T_{film} except for μ_{bulk} and μ_{wall}.

This model is thus an extended correlating equation, with each of the augmentation factors derived using principles and data from the published literature. Each of the above augmentation factors was independently verified against experimental data [9] and the detailed justification for the factors has been presented and discussed by Robinson and co-workers [6, 9].

Using the composite convection model resulted in a mean experimental-to-predicted heat transfer coefficient ratio of 1.06 against a value of 0.29 for the standard DB prediction.

A user-defined subroutine was written into the CFD code to predict the heat transfer coefficient over the heated surface based on this empirical model. It is recognized that this is not a fully analytical solution as this is felt to be beyond the capability of current techniques and resources. Instead this is a pragmatic approach which builds on, and demonstrates continuity with, existing knowledge. The empirical heat transfer equations suggested are based upon global parameters such as hydraulic duct diameter and bulk fluid velocity. To implement this algorithm in a CFD code, some translation of these global parameters to local in-cell values is required. The DB correlation is based on the three dimensionless numbers Nu, Pr, and Re (equation (2)). These can be calculated using the values of thermal conductivity, specific heat capacity, dynamic viscosity, density, and heat transfer coefficient available in each cell. The velocity used

in the Re calculation is the velocity in each cell, and the hydraulic diameter was input as an explicit variable. Using the cell size as a length scale within Re was attempted but the results were found to be divergent.

The modification for developing flow is based on a distance along the duct from the starting location of the fluid dynamic boundary layer. The global position of each cell within the model is known. The global coordinates of the point at which the fluid boundary layer starts has to be explicitly defined in the user subroutine. From this the distance along the duct from the start of the fluid dynamic boundary layer can be determined. The unheated starting length factor is based on the difference between the start of the fluid dynamic boundary layer and the thermal boundary layer. The difference between these starting points also has to be included in the subroutine. The roughness parameter is based on Re and the measured surface roughness and is deduced by an empirical curve fit on a standard Moody [21] diagram. The near-wall fluid viscosity factor is automatically taken care of by using the local cell fluid temperature rather than the bulk fluid temperature, and this is also used in any subsequent calculations that include viscosity.

Figure 9 shows the effect that using all four modifications has on the predicted heat transfer coefficient at a typical test condition of 1 m/s bulk velocity, 90 °C coolant inlet temperature, and 2 bar absolute pressure. Here there is a marked increase in the predicted heat transfer coefficient over the baseline (rough surface wall function) CFD result. All four factors combine to produce a heat transfer coefficient closer to the experimental value.

Table 2 shows the mean heat transfer coefficients for each of the models and the percentage increase over the DB model only. Clearly the entrance factor results in the largest single increase in heat transfer coefficient.

Table 2 Increased heat transfer coefficient in modified convection model (25 mm from the leading edge)

Model	Heat transfer coefficient (W/m² K)	Increase over CFD baseline model (%)
Experiment	11 519	+149
CFD baseline	5343	–
DB only	4064	−12
DB + entrance factor	6103	+32
DB + starting length	5020	+8
DB + viscosity	4702	+1
DB + roughness	5165	+11
DB + all factors	9583	+106

Predicted heat transfer coefficients
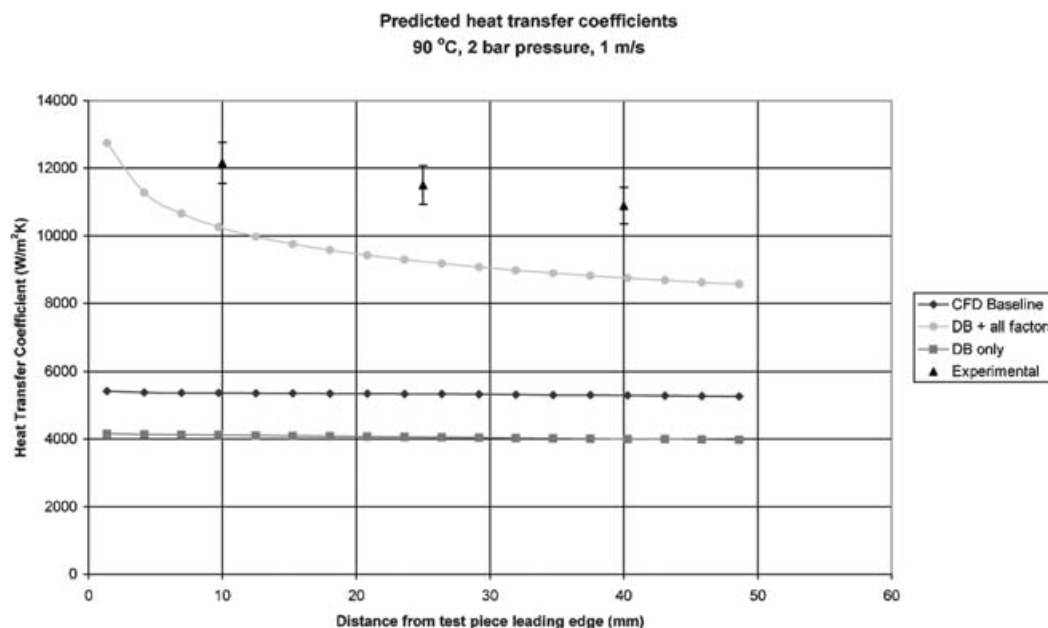**90 °C, 2 bar pressure, 1 m/s**

Fig. 9 Predicted heat transfer coefficients in the convection region, for the DB model and all factors (1 m/s; 2 bar pressure; 90 °C inlet temperature)

The DB empirical equation is based on a Reynolds number derived from the bulk fluid velocity. In the CFD-based approach this velocity is replaced with a local cell velocity, which in the near-wall region is lower than the bulk velocity. For this reason the CFD-based prediction will always give a lower heat transfer coefficient than that predicted by the empirical prediction.

Alternative wall function methods have been recommended that relax the underlying simplifying assumptions given in section 3 [**22**, **23**]. Such formulations may lead to improvements in the prediction of the developing thermal and hydrodynamic boundary layer situation considered here, while retaining most of the economy benefits of the current more empirical treatment.

6 CONCLUSIONS

The use of CFD to model the convective heat transfer in a simulated engine cooling gallery has been described. The convective heat transfer rate is significantly underpredicted using the standard turbulent flow wall function approach, owing to the approximations introduced to simplify modelling of the near-wall region. This is attributed to a combination of inadequate representation of the fluid dynamic boundary layer, the unheated region of the start of the duct upstream of the heated section, the roughness of the heated surface, and the dependence on temperature of the fluid properties.

Alternative modelling approaches have been explored within the CFD environment. Testing of a low-Reynolds-number turbulence model for a fully developed flow case suggests that computing times using this model for the simulation of full engine cooling galleries would be impractical.

An empirical algorithm was introduced to predict the convective heat transfer coefficient using a user-defined subroutine. This was shown to improve comparisons between predicted and measured heat transfer significantly for the cooling gallery experimental rig; however, the method is not easily transferable to other situations.

ACKNOWLEDGEMENTS

REFERENCES

1 **Ennemoser, A., Mahmoud, K.,** and **Winklhofer, E.** Coupled fluid–structure simulation for the thermal analysis of cylinder heads of internal combustion engines. *Motortechnische 2.*, 1999, **60**, 18–20.
2 **Versteeg, H. K.** and **Malalasekera, W.** *An introduction to computational fluid dynamics: the finite volume method*, 1995 (Longman, London).

3 **Leathard, M. J.** *Computational modelling of coolant heat transfer in internal combustion engines.* PhD Thesis, Department of Mechanical Engineering, University of Bath, 2002.

4 **Morgan, R. E., Owen, N. J., Heikal, M. R.,** and **Cox, S. G.** Measurements and prediction of coolant velocity in internal combustion engine cooling systems. In Proceedings of the IChemE Fifth UK National Conference on *Heat transfer,* 1997 (IChemE, London).

5 **Aoyagi, Y., Takenaka, Y., Niino, S., Watanabe, A.,** and **Joko, I.** Numerical simulation and experimental observation of coolant flow around cylinder liners in a V8 engine. SAE paper 880109, 1988.

6 **Robinson, K., Hawley, J. G., Hammond, G. P.,** and **Owen, N. J.** Convective coolant heat transfer in internal combustion engines. *Proc. Instn Mech. Engrs, Part D: J. Automobile Engineering,* 2003, **217**, 133–146.

7 **Robinson, K., Hawley, J. G.,** and **Campbell, N. A. F.** Experimental and modelling aspects of flow boiling heat transfer for application to internal combustion engines. *Proc. Instn Mech. Engrs, Part D: J. Automobile Engineering,* 2003, **217**, 877–889.

8 **Hawley, J. G., Wilson, M., Campbell, N. A. F., Hammond, G. P.,** and **Leathard, M. J.** Predicting boiling heat transfer using computational fluid dynamics. *Proc. Instn Mech. Engrs, Part D: J. Automobile Engineering,* 2004, **218**, 509–520.

9 **Robinson, K.** *IC engine coolant heat transfer studies.* PhD Thesis, Department of Mechanical Engineering, University of Bath, 2001.

10 **Thomas, T. R.** *Rough surfaces,* 1982 (Longman, London).

11 **Nikuradse, J.** Stromungsgesetze in rahen Rohren. *VDI- Forschungsheft,* 1933, **361** (Eng. Transl., NACA Technical Memorandam 1292, National Advisory Committee for Aeronautics, 1950).

12 **Launder, B. E.** Modelling convective heat transfer in turbulent flow – the UMIST approach, IMechE C510/148/95, 1995.

13 **Schlichting, H.** *Boundary layer theory,* 2nd English edition, 1962 (McGraw-Hill, New York).

14 **Apsley, D. D.** and **Leschziner, M. A.** A new low-Reynolds number non-linear two-equation turbulence model for complex flows. *Int. J. Heat Fluid Flow,* 1998, **19**, 209–222.

15 **Wilcox, D. C.** *Turbulence modelling for CFD,* 1993 (DCW Industries, La Canada, California).

16 **Lien, F. S., Chen, W. L.,** and **Leschziner, M. A.** Low-Reynolds-number eddy-viscosity modelling based on non-linear stress–strain/vorticity relations. In Proceedings of the Third symposium on *Engineering turbulence modelling and measurements* (Eds W. Rodi and G. Bergeles), Crete, Greece, 1996, pp. 91–100 (Elsevier).

17 **Dittus, F. W.** and **Boelter, L. M. K.** Heat transfer in automobile radiators of the tubular type. *Univ. Calif. Berkeley, Publns Engng,* 1930, **2**, 443–461.

18 **Boyle, R. J., Spuckler, C. M.,** and **Lucci, B. L.** Comparison of predicted and measured turbine vane rough surface heat transfer. In Proceedings of ASME Turbo Expo 2000, Munich, Germany, 8–11

May 2000, technical paper 2060-GT-0217 (American Society of Mechanical Engineers, New York).

19 **Makkapati, S., Poe, S., Shaikh, Z., Cross, R.,** and **Mikulec, T.** Coolant velocity correlations in an IC engine coolant jacket. SAE paper 2002-01-1203, 2002.

20 **Incropera, F. P.** and **DeWitt, D. P.** *Fundamentals of heat and mass transfer,* 1990 (John Wiley, New York).

21 **Moody, L. F.** Friction factors for pipe flow. *Trans. ASME,* 1944, **66**, 671–684.

22 **Craft, T. J., Gant, S. E., Iacovides, H.,** and **Launder, B. E.** A new wall-function strategy for complex turbulent flows. *Numer. Heat Transfer. Part B: Fundamentals.* 2004, **45**(4), 301–318.

23 **Craft, T. J., Gant, S. E., Gerasimov, A. V., Iacovides, H.,** and **Launder, B. E.** Numerical modelling of heat transfer in wall-adjacent turbulent flows. In *Handbook of numerical heat transfer,* 2nd edition (Eds W. J. Minowycz, E. M. Sparrow, and Y. Y. Murthy), 2006, ch. II (John Wiley, New York).

APPENDIX

Notation

B	constant relating to roughness
D	characteristic length (m)
D_h	equivalent hydraulic diameter (m)
E	constant relating to roughness
k	thermal conductivity (W/m K) or turbulent kinetic energy (J/kg)
k_s	Nikuradse sand roughness (m)
R_a	roughness parameter (μm)
Re_k	roughness Reynolds number
T	temperature (K)
u	component of velocity in the x direction (m/s)
u^+	non-dimensional velocity ($= u/u_\tau$)
u_τ	friction velocity (m/s) $= (\tau_w/\rho)^{1/2}$
x	distance, typically in the direction of flow (m)
x_0	x distance between the start of the velocity boundary layer and the start of the thermal boundary layer (m)
y	distance, typically from the wall (m)
y^+	non-dimensional distance from wall $= yu_\tau/v$
δ	boundary layer thickness (m)
ε	rate of dissipation of the turbulent kinetic energy (m²/s³), or height of the roughness element (m)
κ	constant $= 0.41$
μ	dynamic viscosity (kg/m s)
v	kinematic viscosity (m²/s)
ρ	density (kg/m³)
τ_w	wall shear stress (Pa)